Available online at www.sciencedirect.com
SCIENCE DIRECT®
Journal of Solid State Chemistry 176 (2003) 137–150
JOURNAL OF SOLID STATE CHEMISTRY
http://elsevier.com/locate/jssc

Synthesis, crystal structure and characterization of new 12H hexagonal perovskite-related oxides $Ba_6M_2Na_2X_2O_{17}$ (M = Ru, Nb, Ta, Sb; X = V, Cr, Mn, P, As)

Eric Quarez, Francis Abraham, and Olivier Mentré*

Laboratoire de Cristallochimie et Physicochimie du Solide, UMR CNRS 8012, ENSCL, Université des Sciences et Technologies de Lille, B.P. 108, 59652 Villeneuve d'Ascq Cedex, France

Received 21 March 2003; received in revised form 27 June 2003; accepted 10 July 2003

Abstract

The new $Ba_6Ru_2Na_2X_2O_{17}$ (X= V, Mn) compounds have been prepared by electrosynthesis in molten NaOH and their crystal structures have been refined from single crystals X-ray diffraction, space group $P6_3/mmc$, $Z = 2$, for X= V: a= 5.8506(1)Å, c= 29.6241(4)Å, $R_1 = 4.76\%$, for X= Mn : a= 5.8323(1)Å, c= 29.5299(3)Å, $R_1 = 3.48\%$. The crystal structure is a 12H-type perovskite with a $(c'cchcc)_2$ stacking sequence of $[BaO_3]_c$, $[BaO_3]_h$ and $[BaO_2]_{c'}$ layers. The tridimensional edifice is formed by blocks of Ru_2O_9 dimers that share corners with NaO_6 octahedra. These blocks sandwich double sheets of $X^{5+}O_4$ tetrahedra. Several isotypic $Ba_6M_2^{5+}Na_2X_2^{5+}O_{17}$ materials (X= V, Cr, Mn, P, As) and (M= Ru, Nb, Ta, Sb) have been prepared by solid state reaction and characterized by Rietveld analysis. The magnetic and electric properties have been investigated and show besides the $Ru_2^{5+}O_9$ typical intradimer antiferromagnetic couplings, discrepancies of both χ and ρ versus T at 50 and 100 K for $Ba_6Ru_2Na_2X_2O_{17}$ (X= V, As). In this work, a review of the identified Ru-hexagonal perovskite materials is also reported in order to overview the wide variety of possibilities in the field of new compounds synthesis.

Keywords: Electrosynthesis; Hexagonal Perovskite; Ruthenium oxides; Magnetic properties

1. Introduction

Perovskite-related materials form a wide family, extending from the AMX_3, ideal 3C (C stands for cubic) to various nH or nR (for hexagonal or rhomboedral) polytypes. They are built from anionic layers packing along the c-axis of the hexagonal cell. Both the size of the unit cell and the complexity of the structure are directly related to the n number of independent layers within the periodic sequence. In the field of oxide materials, the large diversity of possible stacked more or less dense layers, i.e., $[O_4]$, $[AO_3]$, $[A_2O]$, $[AO_2]$, $[AO]$…, combined with the diversified packing combinations yield to a huge number of structural types. Furthermore, the network ability to guest a wide variety of chemical species leads to the most important series of investigated synthetic materials in the solid chemistry/physics sciences area. In that field, transition metals have proved to be particularly adapted in regard to the understanding of oxide materials magnetic/electronic properties. Especially perovskite-based materials exhibit characteristics mostly due to metal-oxygen hybridization. Among the available transition metals enabling preparation of new interesting materials, the ruthenium was intensively used, leading to a number of original materials, our work is an additional example of the richness of this research field. An idea of the large diversity of the existing materials is given in Table 1 [1–20] and Table 2 [21–47] which respectively lists the $A_2(B,Ru)_2O_6$ 3C type and 6H type ($BaTiO_3$ type, the most common hexagonal perovskite) perovskite materials with a main Ru mixed or localized valence between +4 and +5.5. It is noteworthy that if several cations such as Ba^{2+}, Ca^{2+}, Sr^{2+}, La^{3+},… are able to form the AO_3 layers of the ruthenium-cubic perovskite, 6H ruthenium phases almost exclusively accept barium in the layers. This is due to the fact that ideal ABO_3 cubic

*Corresponding author. Fax: +33-03-20-43-68-14.
E-mail address: mentre@ensc-lille.fr (O. Mentré).

0022-4596/$ - see front matter © 2003 Elsevier Inc. All rights reserved.
doi:10.1016/S0022-4596(03)00379-7

Table 1
Reported Ru-compounds with 3C type structure classified by decreasing symmetry

Compounds $A_2B_2O_6$	Site A[site B] (cations in parentheses occupy mixed site)	Cell parameters (Å)	Space group	References
$BaLaMnRuO_6$	(BaLa)[(MnRu)]	$a = 3.963$	$Pm\bar{3}m$	[1]
$Ba_2TaRu_{0,5}Na_{0,5}O_6$	Ba_2[($TaRu_{0,5}Na_{0,5}$)]	$a = 4.132$	$Pm\bar{3}m$	[2]
$BaLaFeRuO_6$	(BaLa)[(FeRu)]	$a = 3.973$	$Fm3m$	[3]
$BaLaMgRuO_6$	(BaLa)[MgRu]	$a = 7.957$		
$BaLaCoRuO_6$	(BaLa)[CoRu]	$a = 7.970$		
$BaLaNiRuO_6$	(BaLa)[NiRu]	$a = 7.935$		
$BaLaZnRuO_6$	(BaLa)[ZnRu]	$a = 7.982$		
Ba_2YRuO_6	Ba_2[YRu]	$a = 8.339$	$Fm3m$	[4]
Ba_2LuRuO_6	Ba_2[LuRu]	$a = 8.272$		
$CaLaMnRuO_6$	(CaLa)[(MnRu)]	$a = 5.532, b = 5.477, c = 7.753$	$Pbnm$	[1]
$Ca_3MnRu_2O_9$	Ca_2[($Mn_{2/3}Ru_{4/3}$)]	$a = 5.347, b = 5.463, c = 7.610$	$Pbnm$	[5]
$SrLaCuRuO_6$	(SrLa)[(CuRu)]	$a = 5.604, b = 5.581, c = 7.849$	$Pbnm$	[6]
$SrLaMnRuO_6$	(SrLa)[(MnRu)]	$a = 5.526, b = 5.567, c = 7.816$	$Pbnm$	[7]
La_2NiRuO_6	La_2[(NiRu)]	$a = 5.567, b = 5.595, c = 7.873$	$Pbnm$	[8]
Sr_2CoRuO_6	Sr_2[(CoRu)]	$a = 5.528, b = 5.540, c = 7.830, \beta = 90.21$	$I2/c$	[9]
$SrLaCoRuO_6$	(SrLa)[($CoRu_{0.5}$) ($CoRu_{0.5}$)]	$a = 5.569, b = 5.5680, c = 7.886, \beta = 90.28$	$P2_1/n$	
$BaLaCoRuO_6$	(BaLa)[($CoRu_{0.5}$) ($CoRu_{0.5}$)]	$a = 5.627, b = 5.642, c = 7.986, \beta = 90.12$	$I2/m$	
Sr_2LuRuO_6	Sr_2[LuRu]	$a = 5.740, b = 5.737, c = 8.112, \beta = 90.16$	$P2_1/n$	[4]
Ba_2NdRuO_6	Ba_2[NdRu]	$a = 5.992, b = 5.976, c = 8.448, \beta = 90.02$	$P2_1/n$	[10]
Sr_2YRuO_6	Sr_2[YRu]	$a = 5.769, b = 5.778, c = 8.159, \beta = 90.23$	$P2_1/n$	[11]
Ca_2LaRuO_6	(CaLa)[CaRu]	$a = 5.618, b = 5.837, c = 8.068, \beta = 90.24$	$P2_1/n$	[12]
Sr_2HoRuO_6	Sr_2[HoRu]	$a = 5.771, b = 5.780, c = 8.164, \beta = 90.20$	$P2_1/n$	[13]
Sr_2ErRuO_6	Sr_2[ErRu]	$a = 5.763, b = 5.768, c = 8.149, \beta = 90.19$	$P2_1/n$	[14]
Ca_2NdRuO_6	(CaNd)[CaRu]	$a = 5.556, b = 5.830, c = 8.008, \beta = 90.07$	$P2_1/n$	
Ca_2HoRuO_6	(Ca_1Ho_1)[(Ca_2Ho_2)Ru]	$a = 5.499, b = 5.772, c = 7.938, \beta = 90.18$	$P2_1/n$	
$Sr_3CaRu_2O_9$	Sr_2[$Ca_{2/3}Ru_{4/3}$]	$a = 17.154, b = 5.689, c = 9.863, \beta = 125.0$	$P2_1/c$	[15]
$Ba_3RuBi_2O_9$	Ba_2[$Bi(Ru_{2/3}Bi_{1/3})$]	$a = 6.037, b = 6.049, c = 8.557, \beta = 90.31$	$I2/m$	[16]
Ca_2YRuO_6	(Ca_1Y_1)[(Ca_2Y_2)Ru]	$a = 5.524, b = 5.777, c = 7.964, \beta = 90.23$	$P2_1/n$	[17]
Sr_2FeRuO_6	Sr_2[(FeRu)]	$a = 5.538, b = 5.543, c = 7.877, \beta = 90.11$	$I2/c$	[18]
$BaLaNiRuO_6$	(BaLa)[(NiRu)]	$a = 5.609, b = 5.615, c = 7.957, \beta = 90.16$	$I2/c$	
$BaLaZnRuO_6$	(BaLa)[(ZnRu)]	$a = 5.648, b = 5.667, c = 7.986, \beta = 90.10$	$I2/c$	
Sr_2EuRuO_6	Sr_2[EuRu]	$a = 5.805, b = 5.845, c = 8.230, \beta = 90.36$	$P2_1/n$	[19]
Sr_2GdRuO_6	Sr_2[GdRu]	$a = 5.798, b = 5.832, c = 8.216, \beta = 90.32$	$P2_1/n$	
Sr_2TbRuO_6	Sr_2[TbRu]	$a = 5.788, b = 5.811, c = 8.201, \beta = 90.26$	$P2_1/n$	
Sr_2DyRuO_6	Sr_2[DyRu]	$a = 5.778, b = 5.797, c = 8.182, \beta = 90.27$	$P2_1/n$	
Sr_2TmRuO_6	Sr_2[TmRu]	$a = 5.752, b = 5.753, c = 8.123, \beta = 90.20$	$P2_1/n$	
Sr_2YbRuO_6	Sr_2[YbRu]	$a = 5.743, b = 5.743, c = 8.105, \beta = 90.21$	$P2_1/n$	
Sr_2LuRuO_6	Sr_2[LuRu]	$a = 5.733, b = 5.735, c = 8.097, \beta = 90.18$	$P2_1/n$	
Ba_2PrRuO_6	Ba_2[PrRu]	$a = 6.006, b = 5.986, c = 8.468, \beta = 90.04$	$P2_1/n$	[20]
$Ba_2LaRu_{0,5}Sb_{0,5}O_6$	Ba_2[$La(Ru_{0,5}Sb_{0,5})$]	$a = 6.074, b = 6.089, c = 8.612$	$I\bar{1}$	[2]
		$\alpha = 89.93, \beta = 90.39, \gamma = 89.91$		
Ba_2LaRuO_6	Ba_2[LaRu]	$a = 6.030, b = 6.059, c = 8.537$	$I\bar{1}$	[12]
		$\alpha = 89.86, \beta = 90.33, \gamma = 90.03$		

perovskite requires the Goldsmith factor $t = (r_A + r_O)/\sqrt{2}(r_B + r_O)$ equal to 1. The Ru^V ($r_B = 0.565$ Å in VI coord.) [48] assorted with Ba^{2+} ($r_A = 1.61$ Å in XII coord.) leads to $t = 1.08$, yielding hexagonal packing among close-packed AO_3 layers while smaller A cations respect the cubic structure. The recent focus on the ruthenium emerged for several reasons: (i) This element is especially well adapted to various fruitful preparation routes including the conventional solid state reaction, high pressure treatment under hydrothermal conditions [49,50], or electrosynthesis [51] etc. This last method is being currently developed at the laboratory and is successfully leading to 6H-$Ba_3Ru_2NaO_9$ [46,47] and 10H-$Ba_5Ru_3Na_2O_{14}$ [52] was used in this work. (ii) In the solid state, Ru can adopt a wide range of oxidation number (III, IV, V, VI, VII…) playing a key role in the interplay between electrons and the crystal framework. (iii) Ruthenate has shown unexpected properties such as high-temperature ferromagnetism in $SrRuO_3$ [53], low-temperature superconductivity in Sr_2RuO_4 [54], and non-Fermi liquid behavior in $La_4Ru_6O_{19}$ [55]. Closer to the title materials, several authors studied the magnetic interactions Table 1 [1–20] and within $Ru_2^{5+}O_9$ dimers commonly found in Ru-based hexagonal perovskites. The present work deals with preparation

Table 2
Reported 6H type Ru compounds classified by increasing Ru oxidation state

Compounds	Cations repartition in octahedra $(M/B)O_6$/dimers $(M/B)_2O_9$	Cell parameters a, b, c (Å), α, β, γ (deg)	Space group	References
$BaRuO_3$[a]	RuO_6/Ru_2O_9	$a = 5.71, c = 14.00$	n.g.	[23]
$Ba_3TiRu_2O_9$	$(Ti/Ru)O_6/(Ti/Ru)_2O_9$	$a = 5.715, c = 14.030$	$P6_3/mmc$	[24]
$Ba_3CeRu_2O_9$	CeO_6/Ru_2O_9	$a = 5.889, c = 14.648$	$P6_3/mmc$	[25]
$Ba_3PrRu_2O_9$	PrO_6/Ru_2O_9	$a = 5.885, c = 14.607$		
$Ba_3TbRu_2O_9$	TbO_6/Ru_2O_9	$a = 5.836, c = 14.426$		
$Ba_3InRu_2O_9$	InO_6/Ru_2O_9	$a = 5.839, c = 14.34$	$P6_3/mmc$	[26]
$Ba_3YRu_2O_9$	YO_6/Ru_2O_9	$a = 5.987, c = 14.464$	$P6_3/mmc$	[27]
$Ba_3GdRu_2O_9$	GdO_6/Ru_2O_9	$a = 5.895, c = 14.592$		
$Ba_3YbRu_2O_9$	YbO_6/Ru_2O_9	$a = 5.858, c = 14.432$		
$Ba_3YPt_{0.5}Ru_{1.5}O_9$	$YO_6/(Pt/Ru)_2O_9$	$a = 5.885, c = 14.56$	$P6_3/mmc$	[28]
$Ba_3YPtRuO_9$	$YO_6/(Pt/Ru)_2O_9$	$a = 5.888, c = 14.70$	$P6_3/mmc$	[29]
$Ba_3BiRu_2O_9$	BiO_6/Ru_2O_9	$a = 5.961, b = 10.282$ $c = 14.745, \beta = 91.07$	$C2/c$	[30]
$Ba_3SmRu_2O_9$	SmO_6/Ru_2O_9	$a = 5.914, c = 14.651$	$P6_3/mmc$	[31]
$Ba_3DyRu_2O_9$	DyO_6/Ru_2O_9	$a = 5.880, c = 14.506$		
$Ba_3ErRu_2O_9$	ErO_6/Ru_2O_9	$a = 5.874, c = 14.470$		
$Ba_3SmIrRuO_9$	$SmO_6/(Ir/Ru)_2O_9$	$a = 5.925, c = 14.73$	$P6_3/mmc$	[32]
$Ba_3NdRu_2O_9$ (>120 K)	NdO_6/Ru_2O_9	$a = 5.932, c = 14.759$	$P6_3/mmc$	[33]
$Ba_3LaRu_2O_9$	LaO_6/RuO_6	$a = 5.958, c = 15.006$	$P6_3/mmc$	[34]
$Ba_3EuRu_2O_9$	EuO_6/RuO_6	$a = 5.913, c = 14.637$		
$Ba_3LuRu_2O_9$	LuO_6/RuO_6	$a = 5.854, c = 14.416$		
$Ba_3Mg_{3/4}Ru_{9/4}O_9$	$(Mg/Ru)O_6/Ru_2O_9$	$a = 5.751, c = 14.112$	$P6_3/mmc$	[35]
$Ba_3Zn_{3/4}Ru_{9/4}O_9$	$(Zn/Ru)O_6/Ru_2O_9$	$a = 5.758, c = 14.128$		
$Ba_3NiRu_2O_9$ (5 K)	NiO_6/Ru_2O_9	$a = 5.726, c = 14.060$	$P6_3/mmc$	[36]
$Ba_3ZnRu_2O_9$ (5 K)	ZnO_6/Ru_2O_9	$a = 5.755, c = 14.133$		
$Ba_3CoRu_2O_9$ (5 K)	CoO_6/Ru_2O_9	$a = 5.746, b = 9.918, c = 14.086$	$Cmcm$	
$Ba_3MgRu_2O_9$	MgO_6/Ru_2O_9	$a = 5.765, c = 14.13$	$P6_3/mmc$	[37]
$Ba_3CaRu_2O_9$	CaO_6/Ru_2O_9	$a = 5.900, c = 14.57$		
$Ba_3CdRu_2O_9$	n.g.	$a = 5.875, c = 14.48$		
$Ba_3SrRu_2O_9$	n.g.	$a = 5.925, b = 10.26$ $c = 15.02, \beta = 91.26$	$C2/c$	
$Ba_3InRu_2O_9$	InO_6/Ru_2O_9	$a = 5.818, c = 14.306$	$P6_3/mmc$	[38]
$Ba_3CoRu_2O_9$	CoO_6/Ru_2O_9	$a = 5.751, c = 14.123$		
$Ba_3NiRu_2O_9$	NiO_6/Ru_2O_9	$a = 5.742, c = 14.104$		
$Ba_3FeRu_2O_9$	$(Fe/Ru)O_6/(Fe/Ru)_2O_9$	$a = 5.725, c = 14.065$		
$Ba_3CuRu_2O_9$	CuO_6/Ru_2O_9	$a = 5.672, b = 10.172, c = 14.157$	$Cmcm$	
$Ba_3NiSbRuO_9$	$NiO_6/(Sb/Ru)_2O_9$	$a = 5.786, c = 14.232$	$P6_3/mmc$	[39]
$Ba_3CoIr_{0.25}Ru_{1.75}O_9$	$CoO_6/(Ir/Ru)_2O_9$	$a = 5.753, c = 14.139$	$P6_3/mmc$	[40]
$Ba_3CoIr_{0.5}Ru_{1.5}O_9$	$CoO_6/(Ir/Ru)_2O_9$	$a = 5.756, c = 14.161$		
$Ba_3CoIrRuO_9$	$CoO_6/(Ir/Ru)_2O_9$	$a = 5.755, c = 14.190$		
$Ba_3CoIr_{1.5}Ru_{0.5}O_9$	$CoO_6/(Ir/Ru)_2O_9$	$a = 5.756, c = 14.233$		
$Ba_3CoIr_{1.85}Ru_{0.15}O_9$	$CoO_6/(Ir/Ru)_2O_9$	$a = 5.758, c = 14.269$		
$Ba_3(Ca_{0.8}Sr_{0.2})Ru_2O_9$	$(Ca/Sr)O_6/Ru_2O_9$	$a = 5.907, c = 14.600$	$P6_3/m$	[41]
$Ba_3Ca(Ta_{0.5}Ru_{1.5})O_9$	$CaO_6/(Ta/Ru)_2O_9$	$a = 5.919, b = 14.652$	$P6_3/mmc$	[42]
$Ba_3Ca(Ir_{1.5}Ru_{0.5})O_9$	$CaO_6/(Ir/Ru)_2O_9$	$a = 5.906, b = 14.688$		
$Ba_3SrRu_2O_9$	SrO_6/Ru_2O_9	$a = 5.961, b = 10.305$ $c = 15.076, \beta = 91.18$	$C2/c$	[43]
$Ba_3In_{3/2}Ru_{3/2}O_9$	$(In/Ru)O_6/(In/Ru)_2O_9$	$a = 5.866, c = 14.44$	$P\bar{3}m1$	[26]
$Ba_3Co_{3/2}Ru_{3/2}O_9$	$CoO_6/(Co/Ru)_2O_9$	$a = 5.726, c = 14.059$	$P6_3/mmc$	[44]
$Ba_3Li_{3/4}Ru_{9/4}O_9$	$(Li/Ru)O_6/(Li/Ru)_2O_9$	$a = 5.783, c = 14.192$	$P6_3/mmc$	[35]
$Ba_3NaRu_2O_9$	NaO_6/Ru_2O_9	$a = 5.8729(2), c = 14.4676(7)$		
$Ba_3LiRu_2O_9$	LiO_6/Ru_2O_9	$a = 5.7820(2), c = 14.1490(8)$	$P6_3/mmc$	[45–47]

n.g. stands for information not given in the reference.

[a] At atmospheric pressure, $BaRuO_3$ has the 9R polytype structure [21] which transforms at 15 kbars to the 4H structure [22] and further transforms to the 6H structure at 30 kbars [23]. Finally, a 3C type structure is expected above 120 kbars [23].

and Table 1 [1–20] and characterization of the new $Ba_6M_2^{5+}X_2^{5+}Na_2O_{17}$ series (M = Ru, Sb, Nb, Ta; X = V, Cr, Mn, P, As) Table 1 [1–20] and that crystallize in a 12H type unit cell. The structural and physical properties will be related help and preparation the intensive bibliography published in Table 1 [1–20] and the field.

2. Experimental

2.1. Synthesis

Single crystals of $Ba_6Ru_2Na_2X_2O_{17}$ (X = V, Mn) were grown by electrosynthesis as previously described in connection with preparation of several materials [46,47,51,52,56–61]. NaOH was used as an oxidizing electrolyte, particularly, well suited because of its low melting point (320°C). Then NaOH (pellets), Bi_2O_3, RuO_2, $Ba(OH)_2 \cdot 3H_2O$, V_2O_5/MnO_2 in proportions (g) 10/0.25/0.1/0.5/0.25 were mixed and molten in an alumina crucible batch, set in quartz cell heated at 800°C in a tubular furnace under flowing air. The temperature is controlled at the melt level using a standard K-type thermocouple. In the liquid, a constant potential is applied between nickel and zirconium foils playing the roles of anode and cathode, respectively. After a 24 h reaction, crystals of the title compounds were extracted and water-washed from the deposited material both at the cathode and in the crucible.

Polycrystalline samples of $Ba_6M_2^{5+}Na_2X_2^{5+}O_{17}$ series (M = Ru, Sb, Nb, Ta; X = V, Cr, Mn, P, As) were prepared by the conventional solid state reaction using $BaCO_3$, Na_2CO_3, RuO_2, V_2O_5, MnO_2, $(NH_4)_2HPO_4$, Cr_2O_3, As_2O_5, Nb_2O_5, Ta_2O_5, Sb_2O_3 as starting materials. For most of the materials, an in situ $M^{n+} \rightarrow M^{5+}$ oxidation was expected and effectively achieved. Stoichiometric mixtures of the starting materials were ground in an agate mortar and then heated and reground at 200°C, 400°C and 800°C. Several grinding stages at 800°C are necessary to achieve

Table 3
Crystal data, data collection and structure refinement parameters for $Ba_6Ru_2Na_2X_2O_{17}$ (X = V, Mn)

	V		Mn	
Crystal data				
Symmetry	Hexagonal		Hexagonal	
Space group	$P6_3/mmc$ (no 194)		$P6_3/mmc$ (no 194)	
Unit cell refined on powder (Å)	$a = 5.8506(1)$		$a = 5.8323(1)$	
	$c = 29.6241(4)$		$c = 29.5299(3)$	
Volume (Å^3)	878.17(2)		869.91(2)	
Z	2		2	
Calculated density (g/cm^3)	5.468		5.550	
Data collection				
Equipment	Bruker SMART CCD-1K		Bruker SMART CCD-1K	
Radiation Mo$K\alpha$	0.71073		0.71073	
Scan mode	ω-scan		ω-scan	
Recording angular range 2θ (deg)	2.74–62.72		76–62.76	
Recording reciprocal space	$-8 \leqslant h \leqslant 8$		$-8 \leqslant h \leqslant 8$	
	$-8 \leqslant k \leqslant 8$		$-8 \leqslant k \leqslant 8$	
	$-43 \leqslant l \leqslant 42$		$-42 \leqslant l \leqslant 42$	
Number of measured ref.$[I > 1/2\sigma(I)]$	8103		7285	
Number of independent reflections $[I > 1/2\sigma(I)]$	612		591	
Number of independent reflections $[I > 2\sigma(I)]$	593		512	
μ (mm^{-1}) (pour $\lambda K\alpha = 0.71073$ Å)	15.99		16.54	
Limiting faces and distances (mm)	0 0 1	0.027	0 0 1	0.002
From an arbitrary origin	0 0 $\bar{1}$	0.033	0 0 $\bar{1}$	0.038
	0 1 2	0.031	$\bar{4}$ 0 1	0.012
	2 0 2	0.047	5 0 $\bar{1}$	0.031
	0 $\bar{1}$ 1	0.050	3 2 0	0.029
	$\bar{1}$ 0 1	0.050	$\bar{2}$ 3 3	0.043
	3 $\bar{3}$ 4	0.049	1 $\bar{3}$ $\bar{2}$	0.041
	$\bar{1}$ 1 2	0.040		
Transmission factor range	0.28243–0.43468		0.29478–0.60626	
R merging factor	3.32		5.53	
Refinement parameters				
Number of refined parameters	40		40	
$R_1(F)[I > 2\sigma(I)] = \sum\|\|F_o\| - \|F_c\|\|/\sum\|F_o\|$	4.76		3.48	
$wR_2(F^2)[I > 2\sigma(I)] = [\sum w(F_o^2 - F_c^2)^2/\sum w(F_o^2)]^{1/2}$	8.29		5.28	
$w = 1/[\sigma^2(F_o^2) + (A \times P)^2 + B \times P]$	$A = 0.0000$		$A = 0.0103$	
With $P = [\max(F_o^2 0.0) + 2F_c^2]/3$	$B = 27.5694$		$B = 9.5652$	
Isotropic secondary extinction (type I)	0.00015(5)		0.00092(9)	
Max/Min $\Delta\rho.e$ Å^{-3}	2.39/−1.45		1.52/−1.98	

Table 4
Atomic parameters and isotropic displacement parameters for $Ba_6Ru_2Na_2X_2O_{17}$ with X= V (normal), Mn (*in italics*) from single crystal diffraction

Atoms	Site	Occupancy	x	y	z	U_{eq} (Å^2)
Ba1	4*f*	1	1/3	2/3	0.17907(4)	0.0128(2)
			1/3	*2/3*	*0.17820(3)*	*0.0123(2)*
Ba2	4*f*	1	1/3	2/3	0.59261(3)	0.0128(2)
			1/3	*2/3*	*0.59238(2)*	*0.0117(2)*
Ba3	2*a*	1	0	0	0	0.0251(4)
			0	*0*	*0*	*0.0264(3)*
Ba4	2*b*	1	0	0	1/4	0.0121(3)
			0	*0*	*1/4*	*0.0121(2)*
Ru	4*f*	1	1/3	2/3	0.70468(4)	0.0082(3)
			1/3	*2/3*	*0.70477(3)*	*0.0078(2)*
V	4*f*	1	1/3	2/3	0.05247(9)	0.0089(5)
Mn	*4f*		*1/3*	*2/3*	*0.05253(6)*	*0.0085(3)*
Na	4*e*	1	0	0	0.1245(3)	0.010(1)
			0	*0*	*0.1250(2)*	*0.0078(8)*
O1	12*k*	1	0.177(1)	0.354(2)	0.4268(3)	0.021(2)
			0.1761(7)	*0.352(1)*	*0.4263(2)*	*0.020(1)*
O2	12*k*	1	0.1773(9)	0.355(2)	0.8297(2)	0.014(1)
			0.1775(7)	*0.355(1)*	*0.8299(1)*	*0.013(1)*
O3	6*h*	1	0.512(1)	0.025(2)	1/4	0.009(2)
			0.5125(8)	*0.025(1)*	*1/4*	*0.010(1)*
O4	4*f*	1	1/3	2/3	0.5054(5)	0.033(4)
			1/3	*2/3*	*0.5033(4)*	*0.035(3)*

complete reactions. The purity of the samples was checked by X-ray powder diffraction using a back monochromatized D5000 Siemens diffractometer, λCu$K\alpha$. It is noteworthy that very weak and diffuse lines of $BaCO_3$ are often observed in the final compounds. Results of the syntheses are commented in Section 3.

Electric transport measurements were performed for X= V and As on 2 mm thick pellets shaped with an uniaxial press, and then pressed at 2000 bars using an oil bath isostatic press. Pellets were then sintered at 500°C for a better cohesion. Measurements were performed between 280 and 5 K on a Maglab EXA-DC four-probe apparatus. Colloidal silver paint was deposited on samples and sticked to 50 μm thick gold wires with silver saturated epoxy. The DC current imposed through the two exterior probes is 10 nA. For the resistivity, the l/s (= 5.3 and 4.2 cm^{-1} for $Ba_6Ru_2Na_2X_2O_{17}$ (X= V, As) geometric factor was estimated from the sample shape.

The temperature dependence of the magnetic susceptibility for $Ba_6Ru_2Na_2X_2O_{17}$ (X= V, Cr, As, H = 1000 G; X= Mn, H = 100 G) was measured using a Quantum Design MPMS SQUID magnetometer. $Ba_6Ru_2Na_2P_2O_{17}$ susceptibility was measured using the DC extraction method on an OXFORD Maglab EXA 9T system at H = 10,000 G.

2.2. Single crystal study

Single crystal X-ray diffraction data were collected using a SMART-1K CCD detector BRUKER diffractometer under the conditions given in Table 3. A total of 3 × 600 frames were collected (ω-scans, 10 s. per frame, 0.3° oscillations for three different values of φ : 0°, 120° and 240°) with a crystal-to-detector distance of 45 mm. The intensity data were then extracted from the collected frames using the program Saint Plus 6.02 [62]. An absorption correction based on the faces indexation was then applied using the program Xprep of the SHELXTL package [63]. Data were then corrected for the glass fiber and the area detector absorption using non-theta dependent empirical corrections ($\mu \cdot r = 0$) with the program SADABS [62].

Table 5
Inter atomic distances (Å) and bond valence sums ($\sum S_{ij}$) for $Ba_6Ru_2Na_2X_2O_{17}$ (X= V, Mn) from single crystal diffraction

		V	Mn
Ru^{5+} environment			
Ru–O2	× 3	1.881(6)	1.877(5)
Ru–O3	× 3	2.060(6)	2.052(4)
		$\sum_{ij} S_{ij}$ = 5.04	$\sum_{ij} S_{ij}$ = 5.11
Ru–Ru		2.685(2)	2.671(1)
X^{5+} environment			
X–O1	× 3	1.699(7)	1.707(5)
X–O4		1.71(1)	1.65(1)
		$\sum_{ij} S_{ij}$ = 5.04	$\sum_{ij} S_{ij}$ = 5.05
Na^+ environment			
Na—O1	× 3	2.35(1)	2.337(7)
Na—O2	× 3	2.251(8)	2.234(5)
		$\sum_{ij} S_{ij}$ = 1.56	$\sum_{ij} S_{ij}$ = 1.63

Table 6
XRD powder collection data and Rietveld refinement results for $Ba_6Ru_2Na_2X_2O_{17}$ with X= V, Cr, Mn, P and As

	V	Cr	Mn	P	As
Crystal data					
Symmetry	Hexagonal	Hexagonal	Hexagonal	Hexagonal	Hexagonal
Space group	$P6_3/mmc$ (no. 194)	$P6_3/mmc$ (no. 194)	$P6_3/mmc$ (no. 194)	$P6_3/mmc$ (no. 194)	$P6_3/mmc$ (no. 194)
Unit cell (Å^3)	$a = 5.8508(1)$	$a = 5.8406(1)$	$a = 5.8324(1)$	$a = 5.7851(1)$	$a = 5.8446(2)$
	$c = 29.6247(5)$	$c = 29.5520(5)$	$c = 29.5307(3)$	$c = 29.090(1)$	$c = 29.506(1)$
Volume (Å^3)	878.24(3)	873.04(3)	869.96(2)	843.13(5)	872.87(5)
Z	2	2	2	2	2
Data collection					
Equipment	Siemens D5000	Siemens D5000	Siemens D5000	Siemens D5000	Siemens D5000
Wavelength	Cu$K\alpha_1$, Cu$K\alpha_2$	Cu$K\alpha_1$, Cu$K\alpha_2$	Cu$K\alpha_1$, Cu$K\alpha_2$	Cu$K\alpha_1$, Cu$K\alpha_2$	Cu$K\alpha_1$, Cu$K\alpha_2$
Temperature (K)	300	300	300	300	300
Step scan (deg)	0.02	0.02	0.02	0.02	0.02
Time/step (s)	40	40	40	40	40
Refinement parameters					
Profile function	Pseudo-Voigt	Pseudo-Voigt	Pseudo-Voigt	Pseudo-Voigt	Pseudo-Voigt
Recording angular range 2θ (deg)	5–110	5–110	5–110	5–110	5–110
Number of refined parameters	38	34	31	33	31
Number of reflections	555	551	542	566	566
Zero point	0.0971(9)	−0.0064(8)	0.0099(5)	−0.031(2)	0.011(2)
Profile parameters	$\eta = 1.00000$	$\eta = 0.81(2)$	$\eta = 0.58(2)$	$\eta = 0.91(3)$	$\eta = 1.00000$
	$U = 0.028(2)$	$U = 0.031(2)$	$U = 0.0152(9)$	$U = 0.17(1)$	$U = 0.068(5)$
	$V = -0.009(1)$	$V = -0.013(2)$	$V = -0.0062(7)$	$V = -0.066(9)$	$V = -0.012(4)$
	$W = 0.0036(3)$	$W = 0.0051(3)$	$W = 0.0033(1)$	$W = -0.021(2)$	$W = 0.0067(7)$
	$X = -0.0078(3)$	$X = 0.0027(6)$	$X = 0.0036(4)$	$X = -0.005(7)$	$X = -0.0040(2)$
Asymmetry parameters	Pas 1 = 0.057(7)	Pas 1 = 0.019(6)	Pas 1 = 0.095(5)	Pas 1 = −0.061(7)	Pas 1 = 0.003(7)
	Pas 2 = 0.013(1)	Pas 2 = 0.005(1)	Pas 2 = 0.022(1)	Pas 2 = −0.004(1)	Pas 2 = 0.010(1)
Preferred orientation (March's function)	$G_1 = 0.963(2)$	$G_1 = 0.897(2)$	$G_1 = 0.951(2)$	$G_1 = 1.057(2)$	$G_1 = 0.971()$
Reliability factors					
R_{WP} (%)	11.1	10.1	11.4	10.6	12.7
R_P (%)	8.25	7.82	8.27	8.02	9.31
R_{Bragg} (%)	3.16	4.18	4.84	4.44	3.97
R_F (%)	2.68	3.07	4.14	2.59	3.20
χ^2	1.58	1.61	1.64	1.81	2.27

$R_{WP} = [\sum_i w_i(y_{iobs} - y_{icalc})^2/\sum_i w_i y_{iobs}^2]^{1/2}$.
$R_P = \sum_i |y_{iobs} - y_{icalc}|/\sum_i y_{iobs}$.
$R_{Bragg} = \sum_k |I_{kobs} - I_{kcalc}|/\sum_k I_{kobs}$.
$R_F = \sum ||F_{obs}| - |F_{calc}||/\sum |F_{obs}|$.
$\chi^2 = [R_{wp}/R_{exp}]^2$.

The crystal structure refinement for $Ba_6Ru_2Na_2X_2O_{17}$ with both X= V and Mn was satisfactorily refined in the $P6_3/mmc$ space group using the SHELXTL package [63]. The Patterson function calculation yields the location of four independent barium atoms in two 4(f) sites (1/2, 2/3, $z \sim 0.18$ and $z \sim 0.58$), one 2(a) site (0,0,0) and one 2(b) site (0,0,1/4). Subsequent Fourier difference syntheses lead to the location of complementary Ru, V/Mn, Na and O atoms leading to the title formula. In the last cycles of refinement, anisotropic thermal parameters for all atoms, secondary extinction and an optimized weighting scheme (see Table 3) were considered leading to $R_1/wR_2 = 4.78/8.29\%$ and 3.48/5.28% for the vanadate and the manganate compounds, respectively. The refined atomic coordinates and isotropic displacement parameters are presented in Table 4. The relevant bond lengths with bond valence calculations are listed in Table 5.

2.3. Rietveld analysis

Powder X-ray diffraction data for $Ba_6Ru_2Na_2X_2O_{17}$ (X= V, Cr, Mn, P, As) were collected under the conditions given in Table 6. Impurities resumed in Table 7 were considered in all refinements except for $Ba_6Ru_2Na_2Mn_2O_{17}$ that seems pure at the limit of our X-ray diffraction experiment detection. For all atoms, the initial atomic positions have been taken from the single crystal results obtained for X= V, Mn. FULLROF 2000 was used for powder diffraction data refinements [64]. The atomic coordinates and thermal coefficient refinements indicate no structural difference

Table 7
Refined cell parameters for $Ba_6M_2Na_2X_2O_{17}$ compounds (M = Ru, Nb, Ta, Sb; X = V, Mn, As, Cr, P) and impurities identified by powder XRD

Compounds	a (Å)	c (Å)	Impurities (traces)
$Ba_6Ru_2Na_2V_2O_{17}$	5.8506(1)	29.6241(4)	$BaCO_3$
$Ba_6Ru_2Na_2Cr_2O_{17}$	5.8407(1)	29.5525(2)	$BaCrO_4$
$Ba_6Ru_2Na_2Mn_2O_{17}$	5.8323(1)	29.5299(3)	—
$Ba_6Ru_2Na_2P_2O_{17}$	5.7861(1)	29.0945(7)	$Ba_3(PO_4)_2$
$Ba_6Ru_2Na_2As_2O_{17}$	5.8449(1)	29.5079(8)	$Ba_3(AsO_4)_2/BaCO_3$
$Ba_6Nb_2Na_2V_2O_{17}$	5.866(2)	29.557(8)	—
$Ba_6Ta_2Na_2V_2O_{17}$	5.867(1)	29.533(8)	$Ba_3(VO_4)_2$
$Ba_6Sb_2Na_2V_2O_{17}$	5.925(2)	29.89(1)	$Ba_3(VO_4)_2 + Ba_4NaSb_3O_{12}$
$Ba_6Nb_2Na_2Mn_2O_{17}$	5.872(3)	29.52(1)	—
$Ba_6Ta_2Na_2Mn_2O_{17}$	5.856(3)	29.537(2)	$Ba_3(TaO_4)_2$

between single crystal and powder data. The powder crystal structures were refined because it appears that solid state preparations of polycrystalline samples may lead to significantly different materials from the target-single crystal formulation. Such phenomenon have recently been encountered during our attempts to prepare by solid state reaction the mixed valence 6H-$Ba_3Ru_2^{5.5+}NaO_9$, a KOH flux growth/electrosynthesis product [45,46]. The powder prepared by solid state reaction was in fact, a related 6H-oxycarbonate compound with mixed site Na/Ru that can be formulated $Ba_3(Ru_{1.69}C_{0.31})(Na_{0.95}Ru_{0.05})O_{8.69}$ [47]. Its electro/magnetic properties are largely modified. During the refinements, the oxygen isotropic temperature factors are restrained to be equal to the same value for all compounds. Only for $Ba_6Ru_2Na_2P_2O_{17}$, B_{iso} (Na) is negative, its value is fixed at 0.1 Å^2 value involving a minor increase of R_{Bragg}. The final reliability factors obtained are presented in Table 6. The structural parameters are listed in Table 8 and the relevant bond lengths with bond valence calculation are listed in Table 9. The observed and calculated diffraction patterns and their difference are shown in Fig. 1 conveying a reliable refinement. The possibility of oxygen non-stoichiometry cannot be totally excluded, but is unlikely taking into account the analogy with single crystal data refinements. Furthermore, as observed in all reported compounds of Tables 1 and 2, neither tetrahedra, nor dimers would adopt lacunar coordinations. Considering the V and Mn distances, a good coherence is obtained between single crystal results and less accurate Rietveld results within esd's except for V–O4 (1.71(1) Å versus 1.57(2) Å) and Mn–O4 (1.65(1) Å versus 1.62(1) Å). This divergence is probably due to inaccuracy on O4 location because of its low 4(f) multiplicity.

3. Results and discussion

The most pertinent method of describing hexagonal perovskite materials is based on the stacking of anionic layers. At that point, the recently published wide study reporting structural relationships between these phases is helpful to overview the large possibility of anionic $[A_nO_m]$ layers stacking [65]. In such materials, the occupancy of interstitial sites is essentially guided by the interplay between the kind of layers and the stacking sequence as developed in the following section.

The $Ba_6M_2Na_2X_2O_{17}$ crystal structure is formed by two closely packed blocks of five compact $[BaO_3]$ layer with the (BCACB) sequence, i.e., ($cchcc$). Two blocks are isolated by one $[BaO_2]$ layer, less densely packed to retain the lattice dimensions (Fig. 2). The resulting structure consists of 12 Ba/O layers stacked along the c-axis within a $(c'cchcc)_2$ sequence, where h and c represent hexagonal and cubic $[BaO_3]$ layers, respectively, and c' stands for the cubic $[BaO_2]$ layer (Fig. 3a). This latter is still termed cubic because of its Ba positions and it can be seen as the replacement of a cubic $[BaO_3]$ for an oxygen deficient $[BaO_2]$ layer, leading to isolated tetrahedra pointing towards the central layer (Fig. 3a). This type of stacking is encountered in compounds such as $BaIr_{0.2}Co_{0.8}O_{2.83}$ [66] and $Ba_3V_2\square O_8$ [67]. In contrast, the h' denomination would result from the replacement of an hexagonal $[BaO_3]$ layer, within an ABA block, by a $[BaO_2]$ layer leading to corner sharing tetrahedra pairs (Fig. 3b), as found for example in Ba_2InAlO_5 [68], $Ba_5In_2Al_2ZrO_{13}$ [69] and also $Pb_3Mn_5V_2O_{16}$ [70].

The ruthenium atoms occupy the available O_6 octahedra sites of the (chc) blocks forming commonly observed face sharing Ru_2O_9 dimers.

Dimeric double layers are surrounded by isolated NaO_6 octahedra of the (cc) interstices while the ($cc'c$) tetrahedral sites guest V^{5+}/Mn^{5+} cations. Another way to view the crystal structure from its 3D polyhedral edifice is to consider the well known 6H $(chc)_2$ crystal structure mentioned in Table 2, in which a double slice of tetrahedra would be inserted to isolate the unit-blocks.

Among the number of nH perovskite polytypes, only the recently published 12H-$Ba_6R_2Ti_4O_{17}$ (R = Nd, Y) was found to adopt the same crystal structure that the title compounds with the same $(c'cchcc)_2$ sequence [71]. In these materials R^{3+} and Ti^{4+} are found in the M_2O_9 dimers and corner-sharing octahedra of the ($cchcc$) blocks, instead of Ru^{5+} and X^{5+}, respectively. That leads to $[Ba_5Ti_2R_2O_{15}]^{6+}$ blocks instead of $[Ba_5Ru_2Na_2O_{15}]^{8+}$. Then the double tetrahedral sheets centered around the c' layers are occupied by Ti^{4+} instead of X^{5+}. This coordination is rather unusual for Ti^{4+} and is described by four Ti–O distances (1.70(1) to 1.821(5) Å).

The relative ease of preparation and the analysis of compounds belonging to hexagonal perovskite family made us to consider the M^{5+} substitution for Ru^{5+}, with a similar ionic radius and adopting an octahedral

Table 8
Atomic parameters and thermal parameters for $Ba_6Ru_2Na_2X_2O_{17}$

Atoms	Site	Occupancy	x	y	z	B_{iso} (Å^2)
Ba1	4*f*	1	1/3	2/3	0.17914(7)	1.20(7)
			1/3	**2/3**	**0.17910(6)**	**1.44(5)**
			1/3	*2/3*	*0.17823(5)*	*0.55(4)*
			1/3	***2/3***	***0.17694(9)***	***2.2(1)***
			1/3	2/3	0.17923(8)	1.78(8)
Ba2	4*f*	1	1/3	2/3	0.59285(8)	1.38(7)
			1/3	**2/3**	**0.59247(6)**	**1.51(5)**
			1/3	*2/3*	*0.59238(5)*	*0.68(4)*
			1/3	***2/3***	***0.58835(9)***	***1.28(7)***
			1/3	2/3	0.59210(7)	1.02(6)
Ba3	2*a*	1	0	0	0	2.3(1)
			0	**0**	**0**	**2.21(7)**
			0	*0*	*0*	*1.48(6)*
			0	***0***	***0***	***1.6(1)***
			0	0	0	2.2(1)
Ba4	2*b*	1	0	0	1/4	0.9(1)
			0	**0**	**1/4**	**1.27(7)**
			0	*0*	*1/4*	*0.57(6)*
			0	***0***	***1/4***	***1.8(1)***
			0	0	1/4	0.498(3)
Ru	4*f*	1	1/3	2/3	0.7052(1)	0.86(7)
			1/3	**2/3**	**0.70402(8)**	**1.24(5)**
			1/3	*2/3*	*0.70452(7)*	*0.38(4)*
			1/3	***2/3***	***0.7030(1)***	***2.48(9)***
			1/3	2/3	0.7046(1)	0.97(8)
V	4*f*	1	1/3	2/3	0.0532(2)	1.0(2)
Cr			**1/3**	**2/3**	**0.0523(2)**	**1.6(1)**
Mn			*1/3*	*2/3*	*0.0529(1)*	*0.6(1)*
P			***1/3***	***2/3***	***0.0559(4)***	***0.1(1)***
As			1/3	2/3	0.0537(1)	0.7(1)
Na	4*e*	1	0	0	0.1219(6)	1.2(3)
			0	**0**	**0.1229(4)**	**0.3(2)**
			0	*0*	*0.1243(3)*	*0.5(2)*
			0	***0***	***0.1231(6)***	***0.1******
			0	0	0.1169(5)	0.8(3)
O1	12*k*	1	0.179(3)	0.359(3)	0.4286(4)	1.6(2)[a]
			0.180(2)	**0.360(2)**	**0.4228(3)**	**1.7(1)**[b]
			0.174(2)	*0.348(2)*	*0.4264(3)*	*0.5(1)*[c]
			0.197(2)	***0.394(2)***	***0.4278(4)***	***0.7(2)***[d]
			0.180(3)	0.360(3)	0.4280(4)	1.3(2)[e]
O2	12*k*	1	0.177(3)	0.353(3)	0.8297(4)	1.6(2)[a]
			0.160(2)	**0.320(2)**	**0.8299(3)**	**1.7(1)**[b]
			0.173(2)	*0.346(2)*	*0.8287(3)*	*0.5(1)*[c]
			0.160(2)	***0.320(2)***	***0.8323(4)***	***0.7(2)***[d]
			0.172(3)	0.344(3)	0.8275(4)	1.3(2)[e]
O3	6*h*	1	0.517(4)	0.035(4)	1/4	1.6(2)[a]
			0.500(3)	**0.999(3)**	**1/4**	**1.7(1)**[b]
			0.513(2)	*0.026(2)*	1/4	*0.5(1)*[c]
			0.498(3)	***0.997(3)***	***1/4***	***0.7(2)***[d]
			0.513(4)	0.027(4)	1/4	1.3(2)[e]
O4	4*f*	1	1/3	2/3	0.5000(7)	1.6(2)[a]
			1/3	**2/3**	**0.5051(6)**	**1.7(1)**[b]
			1/3	*2/3*	*0.5019(5)*	*0.5(1)*[c]
			1/3	***2/3***	***0.4977(7)***	***0.7(2)***[d]
			1/3	2/3	0.5036(8)	1.3(2)[e]

X = V (normal), Cr (bold type), Mn (*in italics*), P (*italics bold type*) and As (*underlined*) from Rietveld refinement.
* B_{iso} (Na) = 0.1 Å^2; [a, b, c, d, e] B_{iso} (O_1) = B_{iso} (O_2) = B_{iso} (O_3) = B_{iso} (O_4).

Table 9
Inter atomic distances (Å) and bond valence sums ($\sum S_{ij}$) for $Ba_6Ru_2Na_2X_2O_{17}$ with X= V, Cr, Mn, P and As from Rietveld refinement

		V	Cr	Mn	P	As
Ru^{5+} environment						
Ru–O2	× 3	1.90(1)	2.02(1)	1.89(1)	2.02(1)	1.89(1)
Ru–O3	× 3	2.01(1)	2.17(1)	2.053(8)	2.17(1)	2.05(1)
$\sum_{ij} S_{ij}$ =		5.16	3.57	5.00	3.57	5.01
Ru–Ru		2.654(4)	2.718(3)	2.686(3)	2.734(4)	2.679(4)
X^{5+}environment						
X–O1	× 3	1.65(1)	1.72(1)	1.72(1)	1.45(1)	1.64(1)
X–O4		1.57(2)	1.70(2)	1.62(1)	1.56(2)	1.69(2)
$\sum_{ij} S_{ij}$ =		6.15	6.28	5.05	5.85	5.46
Na^{+} environment						
Na–O1	× 3	2.35(2)	2.27(1)	2.31(1)	2.47(1)	2.25(2)
Na–O2	× 3	2.29(2)	2.14(1)	2.23(1)	2.06(1)	2.39(2)
$\sum_{ij} S_{ij}$ =		1.48	2.04	1.69	1.98	1.50

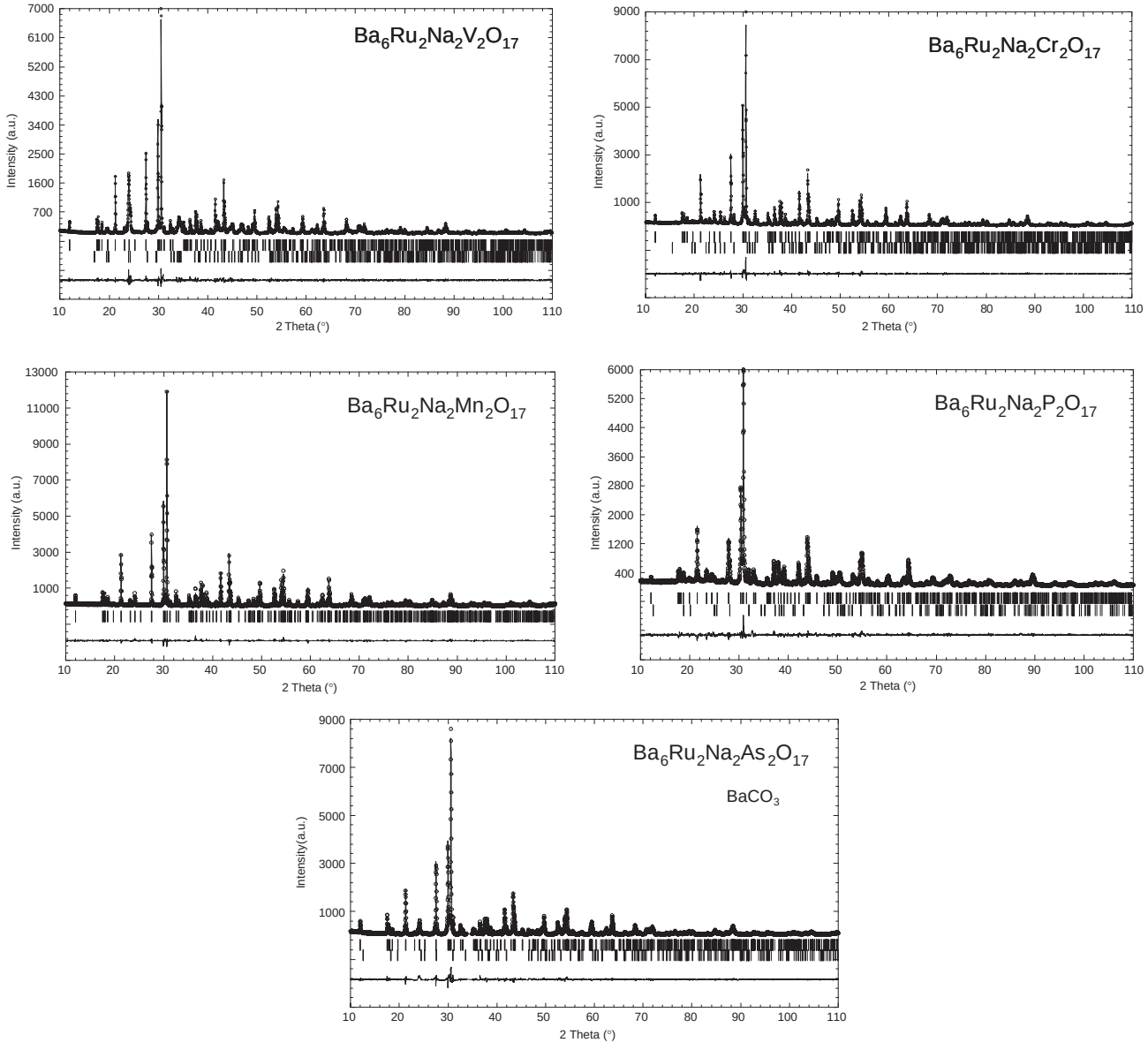

Fig. 1. Observed and calculated XRD patterns and their difference for $Ba_6Ru_2Na_2X_2O_{17}$ (X= V, Cr, Mn, P and As).

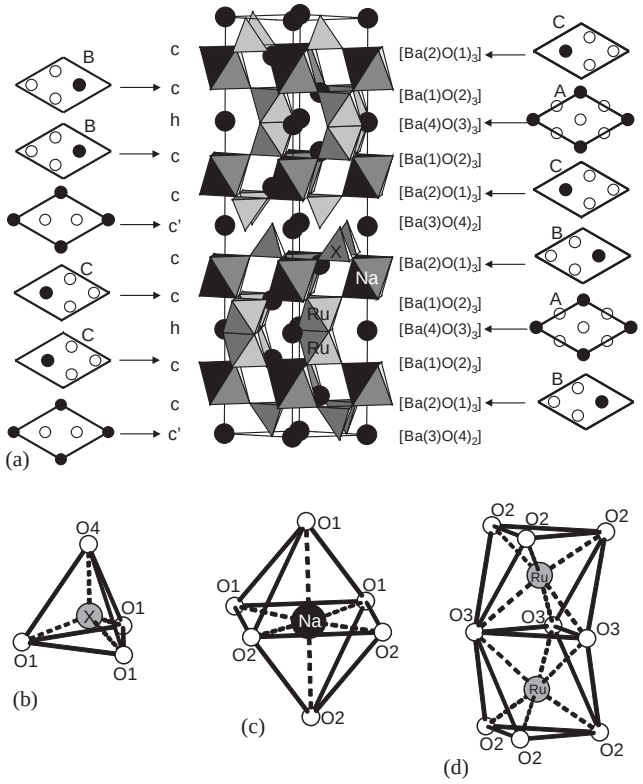

Fig. 2. (a) Structure view of $Ba_6Ru_2Na_2X_2O_{17}$ (X= V, Cr, Mn, P and As) and label of BaO_n layers ($n = 2$ or 3), (b) XO_4 tetrahedra, (c) NaO_6 octahedra and (d) Ru_2O_9 dimer.

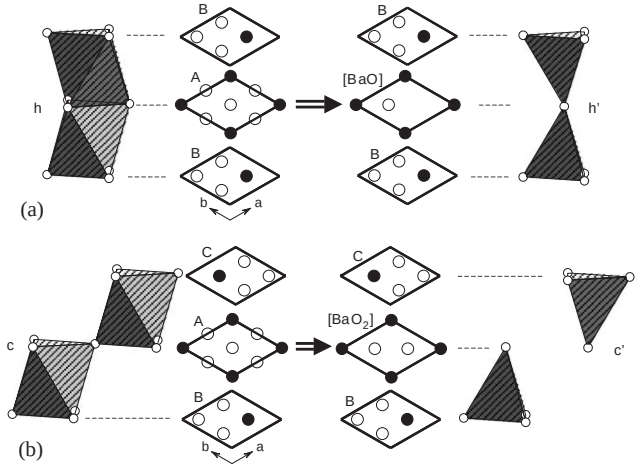

Fig. 3. Schematic representation of polyhedra linkage obtained after replacing a central BaO_3 layer by (a) BaO_2 layer and (b) BaO layer.

environment. The phases $Ba_6M_2Na_2V_2O_{17}$ (M = Nb, Ta, Sb) and $Ba_6M_2Na_2Mn_2O_{17}$ (M = Nb, Ta) were prepared by solid state reaction at 800°C. Only X-ray diffraction and cell parameters refinements have been performed leading to the results reported in Table 7.

3.1. Valence bond sums

3.1.1. Ruthenium

The stoichiometry deduced from structural studies of single crystals and powder compounds lead to a 5+ ruthenium oxidation state in good agreement with successful Nb^{5+}, Ta^{5+}, Sb^{5+} substitutions. The calculated valence bond sum for Ru using the method of Brown and Altermatt method [72] and revised Ru^V data, $r_0 = 1.895$ Å [73], are in good accordance with pentavalent state in the cases of single crystals studies ($\sum S_{ij} = 5.04$ v.u. for V compound and $\sum S_{ij} = 5.05$ v.u. for Mn compound) and of $Ba_6Ru_2Na_2X_2O_{17}$ Rietveld analysis with $X = V(\sum S_{ij} = 5.16$ v.u.), Mn ($\sum S_{ij} = 5.00$ v.u.) and As ($\sum S_{ij} = 5.01$ v.u.). For Cr and P samples, Ru–O distances are longer than commonly observed involving a smaller $\sum S_{ij}$ typical of underbonded cations. The Ru–Ru distances are included in the commonly observed intradimeric distances for Ru^{5+} dimers, i.e., 2.63 Å [74] to 2.78 Å [75]. One can notice that a relationship between Ru–Ru distances and tetrahedral cation size exists. Indeed, tetrahedral pentavalent V, Mn, and As cations are characterized by a nearly similar ionic radius ($r_V = 0.355$ Å, $r_{Mn} = 0.33$ Å and $r_{As} = 0.335$ Å) compared to P^{5+} ($r_P = 0.17$ Å) leading to a drastic decrease of the c lattice parameter. This feature yields greatest Ru–Ru distance in the X= P compound (d Ru−Ru = 2.734 Å) versus X= V, Mn, As (d Ru−Ru ~ 2.67 Å). The $X = Cr^{5+}$ case does not match this observation ($r_{Cr} = 0.345$ Å, d Ru−Ru = 2.718(3) Å) but imprecisions on oxygen coordinates may be involved.

3.1.2. Tetrahedral cation

The oxygen positions imprecisions, as already mentioned for O4, are responsible for the differences observed between X^{5+} valence bond sums calculation from single crystal and Rietveld analysis results. For Mn^V, it is calculated using data deduced from study on $Ba_3Mn_2O_8$ ($r_0 = 1.779$ Å) where Mn adopts a tetrahedral environment [76]. Mn^{5+} (d^2) electronic structure is in favor of $e_g^2t_{2g}^0$ configuration characteristic of a tetrahedral crystalline field and has first been observed in solid materials by Olazcuaga et al. [77] in A_3MnO_4 (A= Na, K) and $ABMnO_4$ (A= Na, K; B = Sr, Ba). For V^{5+}, the value used for valence bond sum $r_0 = 1.7877$ Å [78]. The valence bond sums for both single crystals are very close to the ideal pentavalent state. In the remaining cases, r_0 values are obtained from different studies: for As^{5+}, r_0 (= 1.767 Å) value is indicated in Brese and O'Keeffe work [79]; for Cr^{5+}, r_0 (= 1.882 Å) is calculated from distances observed in $Ba_3Cr_2O_8$ [80] with tetrahedral Cr^{5+} (isotypic with $Ba_3Mn_2O_8$ [76]) and, finally, for P^{5+}, $r_0 = 1.6154$ Å [78]. It appears for these 3 cations that $\sum S_{ij}$ values are greater than

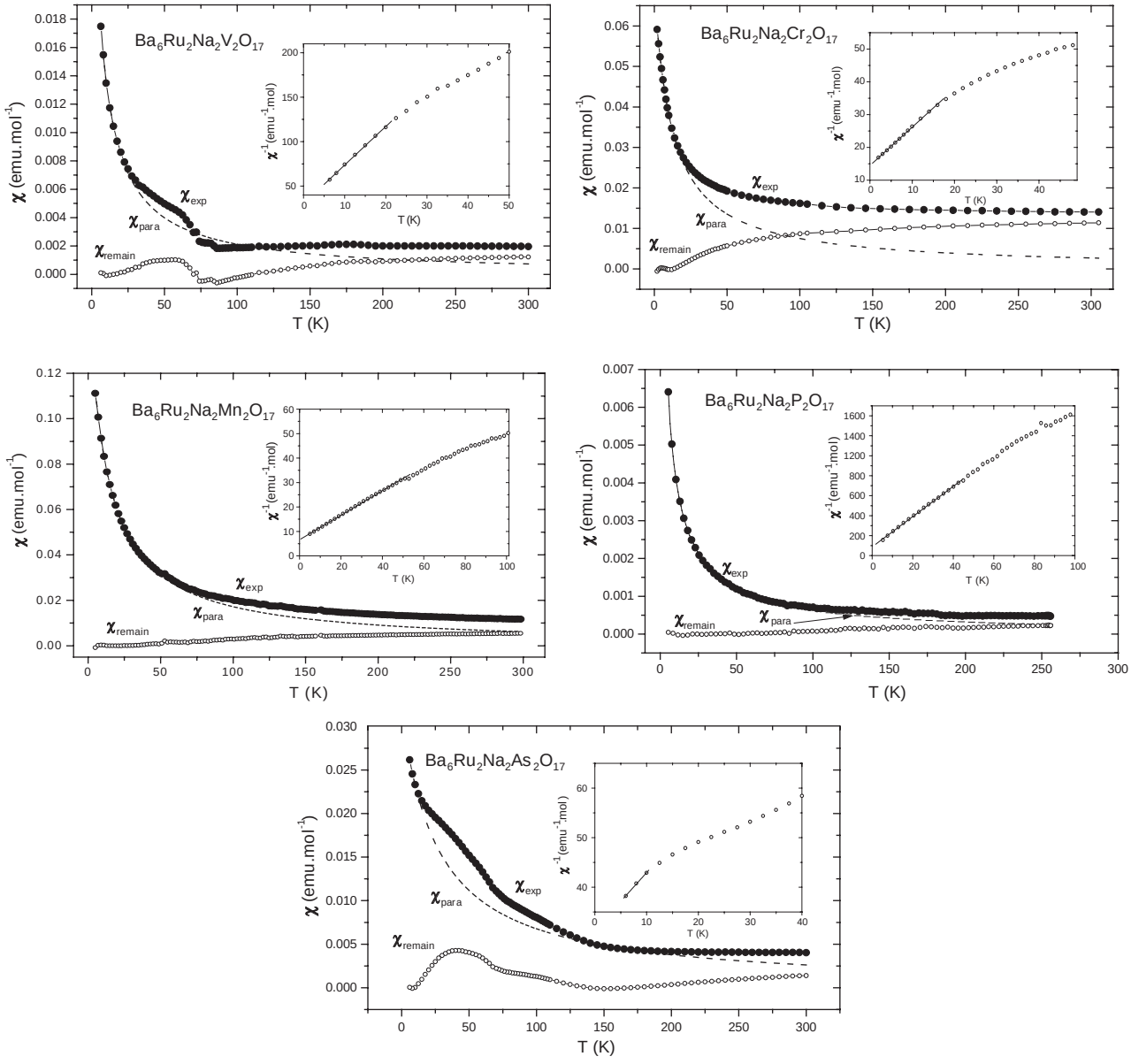

Fig. 4. Temperature dependence of the $Ba_6Ru_2Na_2X_2O_{17}$ (X= V, Cr, Mn, P and As) magnetic susceptibility (χ_{exp}). It also shows the paramagnetic contribution (χ_{para}) fitted from low temperature data (broken line) and their difference, χ_{remain} (white circles). For each curve, the inset shows the χ^{-1} versus T plot and the roughly fitted Curie–Weiss law.

expected. The responsible too short X–O distances may, one more time, suggest oxygen position inaccuracies from powder XRD.

3.1.3. Sodium

For the two single crystal studies and the five Rietveld analysis, it appears that $\sum S_{ij}$ calculated using Brese and O'Keeffe data [79] for the Na^+ cation ($r_0 = 1.800$ Å) are significantly larger than the expected +1 value (1.56 and 1.63 v.u. for V and Mn compounds, respectively, and from 1.48 to 2.04 v.u. for powder samples). This feature was also checked for the recently published 6H-$Ba_3Ru_2NaO_9$ ($\sum S_{ij} = 1.89$ v.u.) [45–47], 10H-$Ba_5Ru_3Na_2O_{14}$ ($\sum S_{ij} = 1.48$ and 1.69 v.u.) [52] and 8H-$Ba_4Ru_3NaO_{12}$ ($\sum S_{ij} = 1.85$ v.u.) [35] which are the only examples of reported perovskite based materials containing octahedral Na and Ru. This rarity may be due to the strong constraints observed for octahedral sodium ($6 \times$ Na–O around 2.25 Å). It appears that Na^+ prefers a prismatic environment such as in Sr_3NaRuO_6, Ba_3RuNaO_6, Ca_3RuNaO_6 [81–83] with $6 \times$ Na–O around 2.35 Å. In fact, by extracting the r_0 value of the $Ba_3Ru_2NaO_6$ material (yielding $r_0 = 1.564$ Å), we obtain very good results for all cases reported above: 0.83 and 0.86 for V and Mn single crystals compounds, respectively; 0.78, 1.08, 0.89, 1.04 and 0.79 and for V, Cr, Mn, P and As powder samples, respectively. So two different values of r_0 should be used for prismatic and

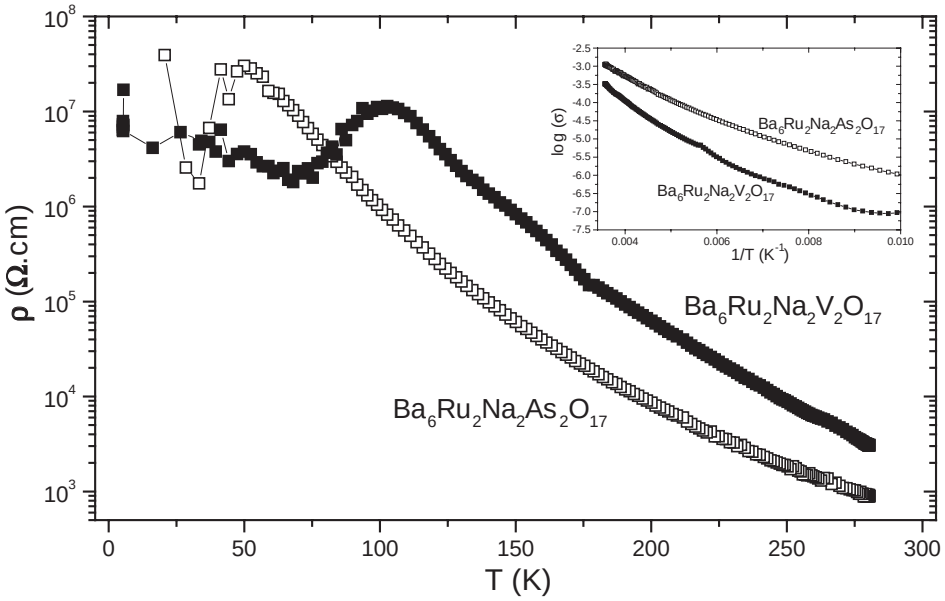

Fig. 5. Resistivity against temperature (log scale) for $Ba_6Ru_2Na_2V_2O_{17}$ and $Ba_6Ru_2Na_2As_2O_{17}$. The inset shows the plot of $\log \sigma = f(T^{-1})$. For X= Cr, Mn and P as soon as room temperature the resistance overflows the maximal detection of the apparatus.

octahedral environment of Na^+ ion. One can notice for P compounds that Na–O distances indicate significantly shift from the center of its $O1_3O2_3$ octahedron towards the $O2_3$ base.

3.2. Magnetic and electric properties

The DC susceptibilities versus temperature for $Ba_6Ru_2Na_2X_2O_{17}$ (X= V, Cr, Mn, P and As) are represented in Fig. 4. For this kind of system, the main magnetic behavior should be composed by the $Ru_2^{5+}O_9$ antiferromagnetic intradimer coupling that can be effective as soon as room temperature and paramagnetic response (intrinsic impurities + paramagnetic $Cr^{5+}(d^1)$ and $Mn^{5+}(d^2)$ when concerned). The paramagnetic contribution fitted with a Curie–Weiss law from the low temperature data lead to the molar Curie constants and the Curie–Weiss temperatures: $Cm_{exp} = 0.84$ K emu ($\theta_{cw} = -12.09$ K) and $Cm_{exp} = 1.93$ K emu ($\theta_{cw} = -12.23$ K) for $Ba_6Ru_2Na_2Cr_2O_{17}$ and $Ba_6Ru_2Na_2Mn_2O_{17}$, respectively. According to a spin-only contribution, the theoretical Curie–Weiss constant related to 2 Cr^{5+}/f.u and 2 Mn^{5+}/f.u are $Cm_{theo} = 0.75$ and 2.0, respectively, values rather close to experimental ones. One should also consider that the fitted values include a part of paramagnetic impurity (possibly of intrinsic origin). It has been estimated for $X = P^{5+}$ and V^{5+}, from low temperature susceptibility data, both being diamagnetic, to $C_{impurity} = 0.066$ and 0.22 K emu, respectively. This last value appears relatively large. For $Ba_6Ru_2Na_2As_2O_{17}$, this estimation is avoided by the lack of linearity in χ^{-1} versus T. The χ_{para} curves were then subtracted from the χ_{exp} curves leading to the χ_{remain} plots (white circles). The χ_{remain} curves should characterize the $Ru_2^{5+}O_9$ magnetic behaviors. Thus, the broad plateau progressively decreasing observed for $X = Cr^{5+}$ and Mn^{5+} is typical of the Ru^V dimers systems, i.e., the energy levels population according to Boltzmann statistic [37]. For $X = As^{5+}$ and V^{5+}, broad anomalies in χ_{remain} appear around 50 and 100 K. Maybe, such phenomena may also exist for Cr^{5+} and Mn^{5+} cases but could be hidden by the relatively large value of the paramagnetic susceptibility. $Ba_6Ru_2Na_2P_2O_{17}$ exhibits a regular plateau, but one should remember that this compound was investigated by the less sensitive DC extraction method for practical convenience. Comparable phenomena (strong ZFC/FC divergence with maxima at 50 and 100 K) have been observed for 6H-$Ba_4Ru_3LiO_{12}$ and assigned to the Li/Ru mixed nature of dimers and corner sharing sites [35]. Our Rietveld experiments did not allow to conclude such a statistical distribution, but it cannot be totally excluded.

We completed this work by a succinct investigation of the resistivity (ρ) and temperature of polycrystalline compounds. For $X = P^{5+}$, Cr^{5+} and Mn^{5+} samples, electrical resistances measured at room temperature are higher than $10^9\,\Omega$, preventing any measurement. For $Ba_6Ru_2Na_2V_2O_{17}$ and $Ba_6Ru_2Na_2As_2O_{17}$ compounds, curves show a progressive evolution from semiconductor to insulator state, Fig. 5. One transition is evidenced at $T = 100$ K for $Ba_6Ru_2Na_2V_2O_{17}$ and at $T = 50$ K for $Ba_6Ru_2Na_2As_2O_{17}$ and may correspond to broad phenomena observed on susceptibility curves (χ_{remain}). Therefore, considering the high values of measured resistances ($\sim 10^8\,\Omega$ at the maximum of the peak), it may

not represent the sample, but due to our 4 probes apparatus even if our system is adapted to measure up to $10^9\,\Omega$ resistances. Attempts to fit an Arrhenius law $\log(1/R) \propto T^{-1}$ did not improve the linearity (inset Fig. 5). Complementary physical properties are currently under investigation and will be reported in a future paper.

Acknowledgments

The authors sincerely thank Dr. E. Gaudin and Dr. J. Darriet, ICMCB, Pessac, France and Dr. C. Marin, CEA, Grenoble, France, for SQUID measurements.

References

[1] A. Horikubi, N. Kamegashira, Mater. Chem. Phys. 65 (2000) 316.
[2] S.A. Almaer, P.D. Battle, P. Lightfoot, R.S. Mellen, A.V. Powell, J. Solid State Chem. 102 (1993) 375.
[3] I. Fernandez, R. Greatrex, N.N. Grennwood, J. Solid State Chem. 32 (1980) 97.
[4] P.D. Battle, C.W. Jones, J. Solid State Chem. 78 (1989) 108.
[5] Z. Serpil Gönen, J. Gopalakrishnan, B.W. Eichhorn, R.L. Greene, Inorg. Chem. 40 (2001) 4996.
[6] M.P. Attfield, P.D. Battle, S.K. Bollen, S.H. Kim, A.V. Powell, M. Workman, J. Solid State Chem. 96 (1992) 344.
[7] A. Horikubi, T. Mori, H. Nonobe, N. Kamegashira, J. Alloys Compd. 289 (1999) 42.
[8] P.D. Battle, C.W. Jones, Mater. Res. Bull. 22 (1987) 1623.
[9] S.H. Kim, P.D. Battle, J. Solid State Chem. 114 (1995) 174.
[10] Y. Izumiyama, Y. Doi, M. Wakeshima, Y. Hinatsu, K. Oikawa, Y. Shimojo, Y. Morii, J. Mater. Chem. 10 (2000) 2364.
[11] P.D. Battle, W.J. Macklin, J. Solid State Chem. 52 (1984) 138.
[12] P.D. Battle, J.B. Goodenough, R. Price, J. Solid State Chem. 46 (1983) 234.
[13] Y. Doi, Y. Hinatsu, K.-I. Oikawa, Y. Shimojo, Y. Morii, J. Mater. Chem. 10 (2000) 797.
[14] P.D. Battle, C.W. Jones, F. Studer, J. Solid State Chem. 90 (1991) 302.
[15] J.T. Rijssenbeek, S. Malo, V. Caignaert, K.R. Poeppelmeier, J. Am. Chem. Soc. 124 (2002) 2090.
[16] J. Darriet, R. Bontchev, C. Dussarrat, F. Weill, B. Darriet, Eur. J. Solid State Inorg. Chem. 30 (1993) 273.
[17] P.D. Battle, W.J. Macklin, J. Solid State Chem. 54 (1984) 245.
[18] P.D. Battle, T.C. Gibb, C.W. Jones, J. Solid State Chem. 78 (1989) 281.
[19] Y. Doi, Y. Hinatsu, J. Phys.: Condens. Matter 11 (1999) 4813.
[20] Y. Izumiyama, Y. Doi, M. Wakeshima, Y. Hinatsu, Y. Shimojo, Y. Morii, J. Phys.: Condens. Matter 13 (2001) 1303.
[21] P.C. Donohue, L. Katz, R. Ward, Inorg. Chem. 4 (1965) 306.
[22] S.T. Hong, A.W. Sleight, J. Solid Sate Chem. 128 (1997) 251.
[23] J.M. Longo, J.A. Kafalas, Mater. Res. Bull. 3 (1968) 687.
[24] D. Verdoes, H.W. Zandbergen, D.J.W. Ijdo, Acta Cryst. C 41 (1985) 170.
[25] Y. Doi, M. Wakeshima, Y. Hinatsu, A. Tobo, K. Ohoyama, Y. Yamaguchi, J. Mater. Chem. 11 (2001) 3135.
[26] H.-U. Schaller, S. Kemmler-Sack, Z. Anorg. Allg. Chem. 473 (1981) 178.
[27] M. Rath, Hk. Müller-Buschbaum, J. Alloys Compd. 210 (1994) 119.
[28] B. Mössner, S. Kemmler-Sack, A. Ehmann, Z. Anorg. Allg. Chem. 487 (1982) 178.
[29] S. Kemmler-Sack, A. Ehmann, M. Herrmann, Z. Anorg. Allg. Chem. 479 (1981) 171.
[30] J. Darriet, R. Bontchev, C. Dussarrat, F. Weill, B. Darriet, Eur. J. Solid State Inorg. Chem. 30 (1993) 273.
[31] H.-K. Müller-Buschbaum, B. Mertens, Z. Naturforsch. B: Chem. Sci. 51 (1996) 79.
[32] I. Thumm, U. Treiber, S. Kemmler-Sack, Z. Anorg. Allg. Chem. 477 (1981) 161.
[33] Y. Doi, Y. Hinatsu, Y. Shimojo, Y. Ishii, J. Solid State Chem. 161 (2001) 113.
[34] Y. Doi, K. Matsuhira, Y. Hinatsu, J. Solid State Chem. 165 (2002) 317.
[35] P.D. Battle, S.H. Kim, A.V. Powell, J. Solid State Chem. 101 (1992) 161.
[36] P. Lightfoot, P.D. Battle, J. Solid State Chem. 89 (1990) 174.
[37] J. Darriet, M. Drillon, G. Villeneuve, P. Hagenmuller, J. Solid State Chem. 19 (1976) 213.
[38] J.T. Rijssenbeek, Q. Huang, R.W. Erwin, H.W. Zandbergen, R.J. Cava, J. Solid State Chem. 146 (1999) 65.
[39] P. Lightfoot, P.D. Battle, Mater. Res. Bull. 25 (1990) 89.
[40] P.D. Battle, J.G. Gore, R.C. Hollyman, A.V. Powell, J. Alloys Compd. 218 (1995) 110.
[41] D. Schlüter, H.-K. Müller-Buschbaum, J. Alloys Compd. 190 (1993) L43.
[42] S. Scheske, H.-K. Müller-Buschbaum, J. Alloys Compd. 198 (1993) 173.
[43] H.W. Zandbergen, D.J.W. Ijdo, Acta Cryst. C 40 (1984) 919.
[44] S.H. Kim, P.D. Battle, J. Solid State Chem. 114 (1995) 174.
[45] K.E. Stitzer, M.D. Smith, W.R. Gemmill, H.-C. zur Loye, J. Am. Chem. Soc. 124 (2002) 13877.
[46] E. Quarez, Ph. D. Thesis University of Lille, 2002.
[47] E. Quarez, M. Huvé, F. Abraham, O. Mentré, Solid State Sci. 5 (2003) 951.
[48] R.D. Shanon, Acta Cryst. A 32 (1976) 751.
[49] C. Renard, S. Daviero-Minaud, F. Abraham, J. Solid State Chem. 143 (1999) 266.
[50] C. Renard, S. Daviero-Minaud, M. Huvé, F. Abraham, J. Solid State Chem. 144 (1999) 125.
[51] H. Samata, M. Furuya, A. Mishiro, Y. Nagata, T. Uchida, M. Ohtsuka, M. Der Lan, J. Phys. Chem. Solids 58 (1997) 1521.
[52] E. Quarez, O. Mentré, Solid State Sci. 5 (2003) 1105.
[53] J.M. Longo, P.M. Raccah, J.B. Goudenough, J. Appl. Phys. 39 (1968) 1327.
[54] Y. Maeno, H. Hashimoto, K. Yoshida, S. Nishizaki, T. Fujita, J.G. Bednorz, F. Lichtenberg, Nature 372 (1994) 532.
[55] P. Khalifah, K.D. Nelson, R. Jin, Z.Q. Mao, Y. Liu, Q. Huang, X.P.A. Gao, A.P. Ramirez, R.J. Cava, Nature 411 (2001) 669.
[56] O. Mentré, A.C. Dhaussy, F. Abraham, E. Suard, H. Steinfink, Chem. Mater. 11 (1999) 2408.
[57] O. Mentré, A.C. Dhaussy, F. Abraham, H. Steinfink, J. Solid State Chem. 140 (1998) 417.
[58] E. Quarez, M. Huvé, P. Roussel, O. Mentré, J. Solid State Chem. 165 (2002) 214.
[59] P. Batail, K. Boubekeur, M. Fourmigué, J.-C.P. Gabriel, Chem. Mater. 10 (1998) 3005.
[60] T.N. Nguyen, Ph.D. Dissertation, Massachusetts Institute of Technology, 1994.
[61] T.N. Nguyen, D.M. Giaquinta, W.M. Davis, H.-C. zur Loye, Chem. Mater. 5 (1993) 1273.
[62] Saint + ver. 5.00, Bruker Analytical X-ray Systems, 1998.
[63] G.M. Sheldrick, SHELXTL NT ver. 5.1, Bruker Analytical X-ray Systems, 1998.
[64] Fullprof 2000, J. Rodriguez-Carjaval, LLB (CEA-CNRS), France, 2000.

[65] J. Darriet, M.A. Subramanian, J. Mater. Chem. 5 (1995) 543.
[66] J.F. Vente, P.D. Battle, J. Solid State Chem. 152 (2000) 361.
[67] A. Durif, Acta Cryst. 12 (1959) 420.
[68] Hk. Müller-Buschbaum, M. Abed, Z. Anorg. Allg. Chem. 591 (1990) 174.
[69] R.V. Shpanchenko, A.M. Abakumov, E.V. Antipov, L.M. Kovba, J. Alloys Compd. 206 (1994) 185.
[70] N. Henry, L. Burylo-Dhuime, F. Abraham, O. Mentré, Solid State Sci. 4 (2002) 1023.
[71] X. Kuang, X. Jing, C.-K. Loong, E.E. Lachowski, J.M.S. Skakle, A.R. West, Chem. Mater. 14 (2002) 4359.
[72] D. Altermatt, I.D. Brown, Acta Cryst. B 41 (1985) 240.
[73] A. Santoro, I. Natali Sora, Q. Huang, J. Solid State Chem. 151 (2000) 245.
[74] D. Schlüter, H.-K. Müller-Buschbaum, J. Alloys Compd. 190 (1993) L43.
[75] C. Dussarrat, J. Fompeyrine, J. Darriet, Eur. J. Solid State Chem. 32 (1995) 3.
[76] M.T. Weller, S.J. Skinner, Acta Cryst. C 55 (1999) 154.
[77] R. Olazcuaga, G. Le Flem, P. Hagenmuller, Rev. Chim. Min. 13 (1976) 9.
[78] F. Zocchi, Solid State Sci. 4 (2002) 149.
[79] N.E. Brese, M. O' Keeffe, Acta Cryst. B 47 (1991) 192.
[80] H. Mattausch, H.-K. Müller-Buschbaum, Z. Naturforsch. B: Anorg. Chem. 27 (1972) 739.
[81] S. Frenzen, Hk. Müller-Buschbaum, Z. Naturforsch. B: Chem. Sci. 50 (1995) 585.
[82] S. Frenzen, Hk. Müller-Buschbaum, Z. Naturforsch. 51b (1996) 1204.
[83] J.B. Claridge, R.C. Layland, R.D. Adams, H.-C. Zur Loye, Z. Anorg. Allg. Chem. 623 (1997) 1131.